Radio Science, Volume 36, Number 4, Pages 681–693, July/August 2001

SOMARE-99: Observations of tropospheric scattering layers using multiple-frequency range imaging

Robert D. Palmer,[1] Phillip B. Chilson,[2,3] Andreas Muschinski,[4] Gerhard Schmidt,[5] Tian-You Yu,[1,6] and Hans Steinhagen[7]

Abstract. Results from an experimental implementation of multiple-frequency range imaging (RIM) are presented. The technique exploits the benefits of frequency diversity to improve range resolution of atmospheric radar systems. The theory has been described in the literature, and simulations have proven its usefulness. Nevertheless, experimental results have been extremely limited. Over a 5-day period in May 1999 we conducted experiments using RIM on the sounding system (SOUSY) radar in northern Germany to observe the layered structure in the troposphere. The experiment is referred to as the SOUSY Multifrequency Atmospheric Radar Experiment 1999 (SOMARE-99). Estimates of range brightness produced by the RIM analysis provide insight about the layered structure of the atmosphere. The RIM results show distinct similarities to previous in situ measurements, which have shown sharp refractive index discontinuities to exist throughout the troposphere and stratosphere. Examples from selected time periods show layers modulated by possible short-period gravity waves or advection of periodic structures as well as other layers with apparent downward motion possibly caused by the progression of a warm front or large-scale subsidence.

1. Introduction

Our ever increasing understanding of the atmosphere creates a desire for high-resolution instrumentation for remote and in situ observations of small-scale atmospheric phenomena. A first glimpse into the submeter-scale reflectivity structure in the atmosphere using radar was provided by *Richter* [1969], who used a frequency-modulated continuous wave (FMCW) radar to observe the lower troposphere. Obvious Kelvin-Helmholtz (KH) waves were seen by these pioneering methods [*Gossard et al.*, 1971]. Recently, in situ instruments with centimeter-scale resolutions have been deployed up to stratospheric heights [*Dalaudier et al.*, 1994]. These balloon-borne measurements have shown the troposphere and stratosphere to be replete with extremely thin (submeter-scale) temperature discontinuities. The relationship between atmospheric radar measurements and these temperature discontinuities was discussed by *Luce et al.* [1995]. Other in situ measurements have been made by using unique observational platforms such as helicopters, kites, and blimps [e.g., *Muschinski and Wode*, 1998]. A comparison has been provided by *Muschinski et al.* [2001a]. These measurements have emphasized that operational, remote-sensing instruments, such as wind profilers, do not have adequate resolution for the observation of these ubiquitous structures. In the current work, we summarize

[1]Department of Electrical Engineering and Center for Electro-Optics, University of Nebraska, Lincoln, Nebraska.

[2]MRI Atmospheric Research Programme, Swedish Institute of Space Physics, Kiruna, Sweden.

[3]Now at the Cooperative Institute for Research in Environmental Sciences, University of Colorado-NOAA, NOAA Environmental Technology Laboratory, Boulder, Colorado.

[4]Cooperative Institute for Research in Environmental Sciences, University of Colorado-NOAA, NOAA Environmental Technology Laboratory, Boulder, Colorado.

[5]Max-Planck-Institut für Aeronomie, Katlenburg-Lindau, Germany.

[6]Now at the National Center for Atmospheric Research, Atmospheric Technology Division, Boulder, Colorado.

[7]Deutscher Wetterdienst, Meteorologisches Observatorium, Lindenberg, Germany.

Paper number 1999RS002307.
0048-6604/01/1999RS002307$11.00

the results from an experimental campaign, using the sounding system (SOUSY) VHF radar in northern Germany, designed to test the feasibility of using advanced radar techniques to overcome this limitation. The experiment is referred to as the SOUSY Multifrequency Atmospheric Radar Experiment 1999 (SOMARE-99).

Typical in situ instruments cannot provide data with sufficient height-time continuity. FMCW radars have good height-time continuity but are limited in altitude coverage to only the lower troposphere. Further, this design of radar does not easily provide Doppler measurements. In contrast, pulsed radar systems can overcome these constraints, but they are burdened by bandwidth restrictions that limit altitude resolution when used in the conventional manner. *Röttger and Schmidt* [1979] used a method of oversampling in range and deconvolution in an early attempt to increase resolution using the SOUSY radar. Another high-resolution method was developed by *Kudeki and Stitt* [1987], who proposed the use of two closely spaced radar frequencies. The technique, termed frequency domain interferometry (FDI), exploited the interference pattern between the coherently detected signals from the two frequencies. Under the assumption that the reflectivity structure within the scattering volume possesses a single, horizontal, Gaussian-shaped layer the cross-correlation function between the two signals can be used to estimate layer altitude and width. Recent work by *Luce et al.* [1999] has helped to put the application of FDI on a solid theoretical foundation. Examples of the successful use of the FDI method for more scientific studies include investigations of an upper level jet stream [*Chilson et al.*, 1997] and large-scale vertical motion [*Muschinski et al.*, 1999].

Even with the success of two-frequency FDI, the underlying assumption that only a single Gaussian-shaped layer exists within the scattering volume has been a concern. In fact, *Franke* [1990] proposed the use of more than two transmitter frequencies. However, no experimental data were presented to verify the theory. *Palmer et al.* [1999] showed that Franke's "pulse compression" viewpoint results in a formula that is the Fourier transform of the set of correlation functions from all signal combinations of the multiple frequencies. This method is approximately equivalent to the Fourier-based range imaging (RIM) technique in which the Fourier transform of the visibility matrix produces an estimate of the so-called range brightness [*Palmer et al.*, 1999; *Luce et al.*, 2001]. The visibility matrix, denoted by $\mathbf{V}(f)$, where f is the temporal frequency, has elements spanning the available spatial samples of the continuous visibility function. It should be mentioned that the work of *Palmer et al.* [1999] and *Luce et al.* [2001] occurred simultaneously and independently and that both groups concluded that RIM has potential to reveal the fine structure in the atmosphere. Note that *Luce et al.* [2001] refer to the technique as frequency domain radar interferometric imaging (FII).

The range brightness is the normalized distribution of power within the scattering volume along the boresight of the radar. Although the Fourier-based RIM technique can be used to probe the reflectivity structure within the scattering volume, its resolution was shown to be insufficient for observational implementation. However, in many ways the RIM technique is similar to estimating the angular brightness distribution using coherent radar imaging (CRI) [*Kudeki and Sürücü*, 1991]. In the CRI method, several spatially separated receivers are placed at the surface to sample the spatial correlation function. The CRI method is well known and has been used in the radio astronomy community for some time [e.g., *Thompson*, 1986]. Recently, the method has been used for atmospheric radar applications, and several techniques have emerged to solve the rather difficult CRI inverse problem [e.g., *Hysell*, 1996; *Woodman*, 1997; *Palmer et al.*, 1998].

By using the connection between CRI and RIM, *Palmer et al.* [1999] showed that the range brightness distribution could be estimated with such a significant improvement in resolution that fine details in the reflectivity structure could be examined. The improvement was obtained by using a constrained optimization approach, similar to that originally proposed by *Capon* [1969]. The approach was verified by using numerical simulations but no experimental data were provided [*Palmer et al.*, 1999].

Here, we summarize the results from SOMARE-99 which was designed to test the capability of RIM. Instrumental components of the campaign included the SOUSY VHF radar in northern Germany, four spatially separated microbarographs, and radiosonde launches every 3 hours during the almost week-long campaign. Results from the correlative instruments are presented by *Chilson et al.* [this issue] and *Muschinski et al.* [2001b].

2. Fundamentals of Range Imaging

As in standard two-frequency FDI analysis, RIM is implemented by changing the transmitter frequency from pulse to pulse. Upon reception, the received signals are coherently detected and integrated to produce the signals $s_1(t)$, $s_2(t)$, ..., $s_m(t)$, where m is the number of frequencies. In the case of two-frequency FDI, however, m is set to only 2. Of course, the decorrelation time of the Bragg-scale scatterers must be longer than the time needed to cycle through the m frequencies. The visibility matrix $\mathbf{V}(f)$ can be easily constructed from the m signals by calculating and normalizing all combinations of temporal autospectra and cross-spectra. *Palmer et al.* [1999] showed that the range brightness could then be estimated by a Fourier transform of the visibility functions, resulting in the equation

$$\hat{B}_{rF}(r_I, f) = \mathbf{e}_r^{\dagger}\mathbf{V}(f)\mathbf{e}_r, \tag{1}$$

where the dagger denotes the Hermitian operator and the "range steering vector" is

$$\mathbf{e}_r = \left[\; e^{-j(2k_1 r_I - \phi_1)} \quad \ldots \quad e^{-j(2k_m r_I - \phi_m)} \;\right]^T. \tag{2}$$

The wavenumbers corresponding to each of the m signals are denoted by k_i for signal i. By scanning r_I, which is the desired range to be imaged, throughout the gate, an estimate of the range brightness distribution can be obtained as a function of position within the volume. From (2) it is important to note that the technique attempts to phase lock the m signals at range r_I, which is then varied within the range gate. Important components in (2) are the initial phase terms ϕ_i. Without knowledge of the initial phase of each signal, or at least the phase difference between each signal pair, the steering vector cannot accomplish the task of phase locking the m signals at range r_I. As a result, the summation produced in (1) would not be coherent. However, if the initial phase terms are known or negligible, the details of the echo power within the range gate can be revealed.

Estimating the range brightness from (1) is equivalent to taking a discrete Fourier transform of the sampled visibility functions. Such a procedure has well known resolution characteristics, which limit the usefulness of the Fourier-based RIM analysis for atmospheric studies. As mentioned in Section 1, *Palmer et al.* [1999] used an inversion technique based on constrained optimization to produce the following Capon range brightness estimate:

$$\hat{B}_{rC}(r_I, f) = \frac{1}{\mathbf{e}_r^{\dagger}\mathbf{V}^{-1}(f)\mathbf{e}_r}. \tag{3}$$

Using simulations, this implementation of RIM was proven to be capable of exposing the fine structure of the echo power distribution within the scattering volume. Other types of inversion methods, such as maximum entropy, could be used to solve the problem but are more computationally expensive. Nevertheless, these methods have been used for CRI studies of the angular brightness distribution in the ionosphere [e.g., *Hysell*, 1996], as well as in statistical studies using simulations [*Yu et al.*, 2000].

3. Experimental Configuration and Phase Calibration

The experimental implementation of RIM used the SOUSY VHF radar located in the Harz mountains of Germany (51.66°N, 10.49°E). Characteristics of the radar include a 72-m aperture and flexible beam steerability. The transmitter uses a linear amplifier with 600-kW peak pulse power, bandwidth of 2.5 MHz, and 4% duty cycle. A detailed description of the radar is given by *Schmidt et al.* [1979] and *Czechowsky et al.* [1984].

A major goal of SOMARE-99 was the detailed comparison of the layered structure in the free troposphere with the dynamics of the wind field. Therefore it was essential to have periodic estimates of the wind profile. The standard Doppler beam swinging (DBS) procedure was employed for this purpose with a single transmitter frequency of 53.5 MHz, which is the nominal frequency for the SOUSY radar. Returned signals from the complementary coded (4-bit), 2-μs rectangular subpulses were sampled every 300 m from 2.35 to 8.35 km above mean sea level (msl). An interpulse period (IPP) of 200 μs was used with 200 coherent integrations. Including processing delays, an effective sampling time of 0.0493 s resulted. Therefore the aliasing velocity was 28.44 m s^{-1}, which was more than adequate for the expected tropospheric winds. A 512-point data set was obtained for the vertical beam direction; then, the beam was successively steered in the four cardinal directions (N-S-E-W) with a zenith angle of 7°. Operating parameters for the oblique beams were identical to those for the vertical beam. One cycle of the five-beam DBS portion of the experiment was completed approximately every 2.1 min. It should be noted that at VHF wavelengths the use of a zenith

angle of 7° for wind measurements could show effects of aspect sensitivity. These would be characterized by a slight underestimate of the horizontal wind magnitude caused by a shift toward zenith of the effective pointing angle. Such small errors have not be accounted for in this study.

The DBS cycle was alternated with a vertical beam, multiple-frequency (MUFR) mode; resulting data were used for the RIM implementation. The four frequencies used were 53.25 MHz, 53.33333 MHz, 53.58333 MHz, and 53.75 MHz, which are centered about the nominal frequency of the radar. Frequencies were shifted after every complementary code cycle, which included a code flip for direct current (dc) signal removal. The nonuniform frequency spacing was chosen to reduce redundancy in the frequency lags available from the data. Such spacings are often implemented in sparse antenna array design to produce grating lobes with larger separation [e.g., *Johnson and Dudgeon*, 1993]. Of course, the trade-off is the production of higher-range sidelobes than what would be obtained using uniform spacing, but this problem is mitigated by the adaptive nature of the Capon algorithm given in (3).

The rectangular 2-μs subpulses produce a transmit bandwidth of approximately 500 kHz, and with the span of the four frequencies mentioned above, the overall bandwidth of the experiment is 1 MHz. The receiver has a bandwidth of 1 MHz which accommodates the signals without distortion. Baseband, decoded signals are passed through a Bessel matched filter with 500-kHz bandwidth providing optimal noise suppression. Since this MUFR experiment uses a total bandwidth of 1 MHz, the question that should be answered is whether the RIM analysis can provide resolution better than that which would be obtained using 1-μs pulses matched to the total bandwidth. Note that previous work using numerical simulations has shown that Capon RIM does improve resolution over conventional methods, while this is not the case for Fourier RIM [*Palmer et al.*, 1999].

Range sampling was the same as in the DBS mode but with three additional gates placed at 14.35 to 14.95 km msl for phase calibration. An ultrasonic delay line was used to leak the transmitted signal directly back to the receiver without atmospheric modification at a range of approximately 14.65 km msl. Note that the atmospheric returns at this altitude are extremely weak. Therefore the delayed signal was stable and easily detectable in the data. Since the signal is due almost solely to the transmitter, the phase difference among the four signals could be used to compute the initial phase terms in (2). This calibration procedure proved to be robust and easy to implement although the estimated initial phase terms were extremely small. Except for relatively small system phase differences, the demodulation process removes the majority of the random phase offset. As a result, the main purpose of the calibration procedure is the determination of absolute range.

The MUFR mode used the same IPP of 200 μs but with 500 coherent integrations. Including the alternation of the four frequencies and processing delays, an effective sampling time of 0.4374 s was obtained. Since only a vertical beam was used for the MUFR mode, the resulting 3.21 m s^{-1} aliasing velocity was appropriate. Again, 512 time series points were collected, but these data correspond to interlaced signals from the four frequencies. Therefore each separate time series (record) consisted of 128 points. Fifteen records of MUFR data were recorded before cycling back to the DBS mode, resulting in a total cycle time of approximately 16.2 min for both modes.

The DBS and MUFR modes were alternated during the experiment, which began at 1445 UT on May 24, 1999. Except for relatively short system failure periods the data were continuously collected until 2017 UT on May 27, 1999. Note that the experiment was actually continued until 1539 UT on May 28, 1999, but only in the DBS mode. The extended data set obtained is examined by *Chilson et al.* [this issue] and *Muschinski et al.* [2001b].

4. Experimental Results

Using data from the DBS portion of the experiment, we calculated the zonal and meridional components of the horizontal wind from the radial velocity estimates determined by the five beam positions. The zero-frequency components of radar Doppler power spectra are typically contaminated by unwanted contributions from ground clutter and/or instrumental offsets/biases. In the present case, these contributions are removed in two stages. First, the dc signals for each beam record were removed from the in-phase and quadrature channels separately. Second, the zero-frequency components of power spectra were replaced with the average of the adjacent

frequency bins. When dealing with the MUFR data, the same procedure was applied separately for each of the four signals. Prior to performing a discrete Fourier transform on the data in order to calculate the power spectra, the time series were weighted with a Hanning window. The stronger spectral leakage associated with use of a rectangular window was found to lead to overestimations of the noise level [*Hooper*, 1999].

An accurate calculation and removal of the noise floor is critically important to assure reliable estimates of the first three moments of the Doppler spectrum. *Petitdidier et al.* [1997] discuss different methods of evaluating and removing noise from spectra and their respective advantages. We have chosen to apply their segment method to the outermost quarters of the Doppler spectra. Considering that the Nyquist velocity was as large as 28.44 m s^{-1}, the segment method offered a simple and effective method of estimating the noise floor. The noise level was determined and removed separately for each spectrum. Whereas sky noise is expected to be constant over all sampling heights, instrumental effects such as slow receiver recovery times could create noise levels that show a height dependence.

After removal of the noise the signal parameters, echo power, Doppler velocity, and spectral width were calculated using the moments method [*Woodman*, 1985]. The sense of the Doppler shift was chosen such that motion away from the radar is given by positive values. When operating in the MUFR mode, the Doppler velocities were simply interpreted

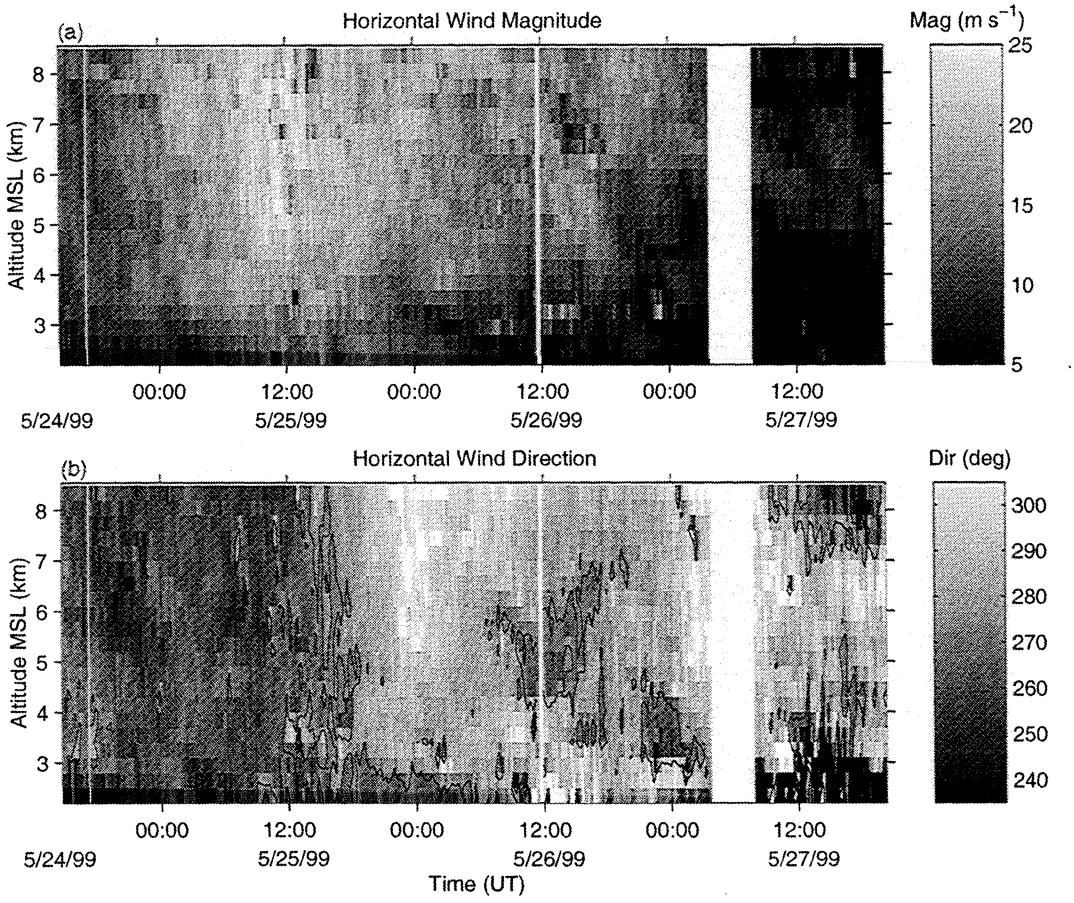

Figure 1. Profiles of (a) magnitude and (b) azimuth angle of the horizontal wind vector, estimated by using a five-beam DBS procedure. Note the wind maximum at 1200 UT on May 25, 1999, at an altitude of approximately 8 km msl. A single contour line has been placed at an azimuth angle of 270°, emphasizing the transition from a southwesterly to a northwesterly flow.

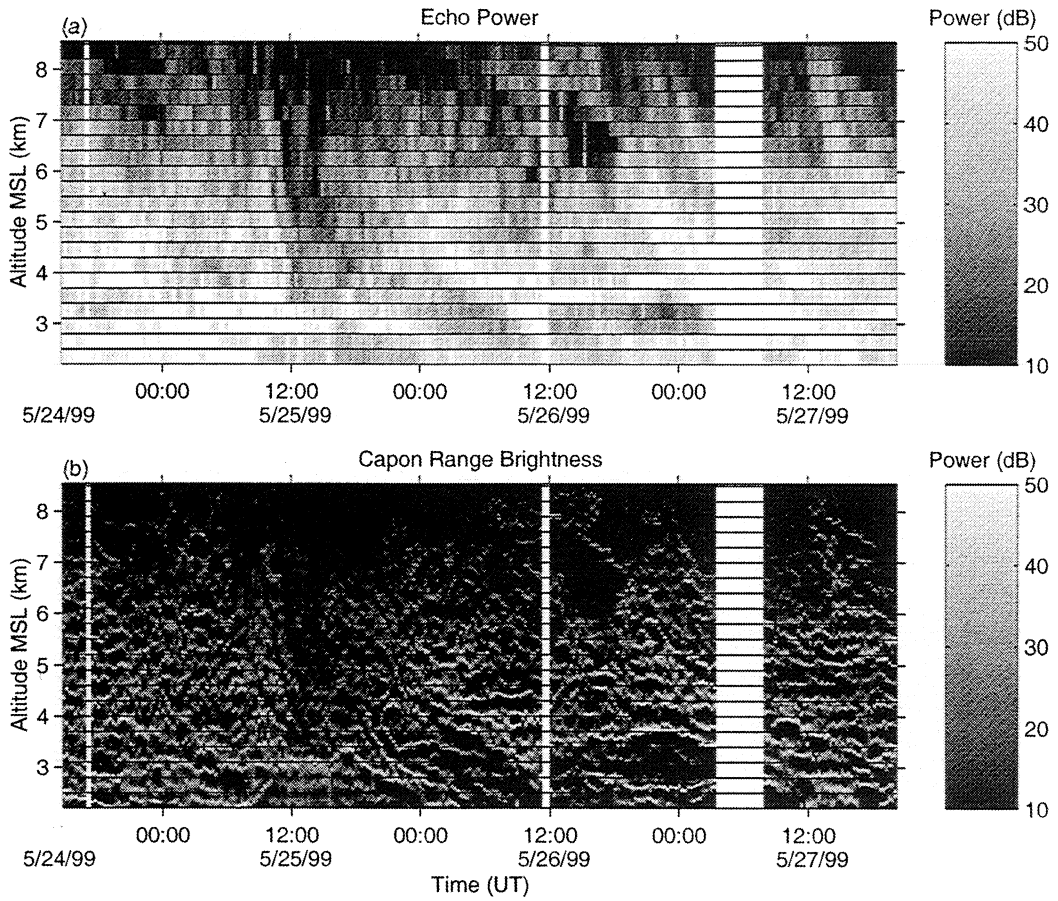

Figure 2. Profiles of (a) standard echo power and (b) power-weighted range brightness obtained by using the Capon RIM technique. Fifteen incoherent integrations were performed providing a temporal resolution of approximately 16 min. Horizontal lines are shown to emphasize the boundaries between the 21 gates. The altitude ranges from 2.35 to 8.35 km msl with a 300-m gate spacing.

as being the vertical velocity. The zonal, meridional, and vertical components of the wind were estimated from the DBS records by solving the overdetermined matrix equation using a least squares analysis. The computed magnitude and azimuth angle of the horizontal wind vector were then calculated and are shown in Figure 1. Note that the azimuth angle corresponds to the direction from which the wind originates. A wind maximum is seen to pass over the radar site at approximately 1200 UT on May 25 at an altitude of at least 8 km msl. Synoptic weather maps, described in our companion paper [*Chilson et al.*, this issue], show that the observed wind maximum was due to the passage of an upper level trough associated with the Icelandic low. The maximum westerly flow observed by the radar was approximately 30 m s^{-1}. From the azimuth angle estimates in Figure 1b the horizontal wind is seen to change from a southwesterly to a northwesterly flow at the same time as the occurrence of the wind maximum. To emphasize the location of purely zonal flow, a single azimuth angle contour line is shown for 270°.

Echo power was estimated by the zeroth moment of the vertical beam Doppler spectrum (shown in Figure 2a) over the extent of the experiment. Solid, horizontal lines are shown at the gate boundaries, which are 300 m apart. During the wind maximum the echo power is seen to decrease at the peak location. This characteristic is most likely due to the lack of vertical shear in the horizontal wind exactly at

the peak. Of course, large shear would be expected immediately surrounding the wind maximum, which could, in turn, produce dynamic instabilities.

As mentioned in Section 3, for each cycle of the experiment, fifteen 128-point records of MUFR data were obtained for each of the four frequencies. An approximate 16-min temporal resolution was obtained by incoherently integrating 15 temporal autocorrelation and cross-correlation functions, from which the zero-lag value was extracted and used to construct the visibility matrix. This procedure is much more computationally efficient but does not allow studies of the differences in range brightness for various Doppler frequencies. The visibility matrix was then used to estimate the Capon range brightness for the entire data set. Range brightness, which varies from zero to 1, was then multiplied by the echo power (dB) in order to provide a composite picture of the layered structure and the echo power. These data are shown in Figure 2b, again, with the gate boundaries emphasized by solid, horizontal lines. Each gate was segmented into 60 subgates by varying r_I in (2), providing a range sampling of 5 m. It should be emphasized that the range resolution is not 5 m, but only the range sampling. Although Capon's method has been proven to possess much better resolution than Fourier-based methods, its actual resolution depends on the particular reflectivity structure of the atmosphere. As a result, resolution is rather difficult to quantify, although *Palmer et al.* [1999] attempted to do so by using simulation methods. The effect of the range weighting function was removed by dividing the estimated range brightness by a Gaussian function with second central moment given by $\sigma_r = 0.35c\tau/2$ (for a Gaussian filter matched to a rectangular pulse) [*Doviak and Zrnić*, 1984]. Here c is the speed of light, and τ is the radar pulse length. When calculating the range brightness, we have chosen to adopt a slight modification to this model. To avoid sharp discontinuities at the range gate boundaries, the slope of the range weighting function has been forced to zero at these locations. Note the distinct layering structure revealed throughout the troposphere when using Capon RIM. After the wind maximum, for example, several intense layers are observed in the 3-5 km msl range, where an apparent downward motion persists for many hours.

To gain further confidence in the results obtained with the RIM technique and to provide an initial comparison, the range brightness was estimated by both the Fourier and Capon RIM methods. In addition, standard two-frequency FDI analysis using the signals from frequencies 53.25 and 53.75 MHz provided an estimate of layer position and thickness. When using two-frequency FDI analysis, we assume that only a single Gaussian layer exists within each range gate. Nevertheless, two-frequency FDI is an established method and should be used for comparison. Using no incoherent integration, we estimated the visibility matrix again and obtained an improved temporal resolution of approximately 1 min. An interesting example from all three methods is shown in Figure 3 for the ranges 3.65-4.25 km msl for a 3.5-hour period. The data, which begin at 0730 UT on May 26, 1999, show the superposition of at least two coherent wavelike structures. The source of these patterns could be due to gravity wave oscillation or the advection of periodic structures, such as KH billows, although the period does not support the latter hypothesis. Notice that the Fourier RIM results, shown in Figure 3a, do not possess the detail necessary to easily recognize the coherent structure. Furthermore, the two-frequency FDI layer position (shown as a heavy solid line) and layer thickness (shown as error bars) follow the peak in the Fourier range brightness, but transitions through gate boundaries are difficult to interpret. Note that the FDI implementation used here, from the pioneering work of *Kudeki and Stitt* [1987], is extremely simple, but it does not take into account the biases caused by the range weighting function. As a result, the two-frequency FDI layer position estimates are shifted slightly away from the peak in the Fourier RIM brightness distribution. Estimates of the layer position could be improved by using more recent developments in the FDI technique, but this is not the focus of the current work. As expected, the range brightness estimated by the Capon RIM method has distinct similarities to that obtained by both the Fourier RIM and two-frequency FDI analyses, but its resolution is superior, allowing the details of the structure to be easily discerned. Details of a simulation study of the resolving capabilities of Capon RIM were provided by *Palmer et al.* [1999]. Since the only normalization induced on the range brightness distributions is that of the echo power, the differences in the brightness maps from Fourier and Capon RIM are real and not a manifestation of some normalization procedure. Concentrating on the Capon RIM results in Figure 3b, the wavelike structure is seen

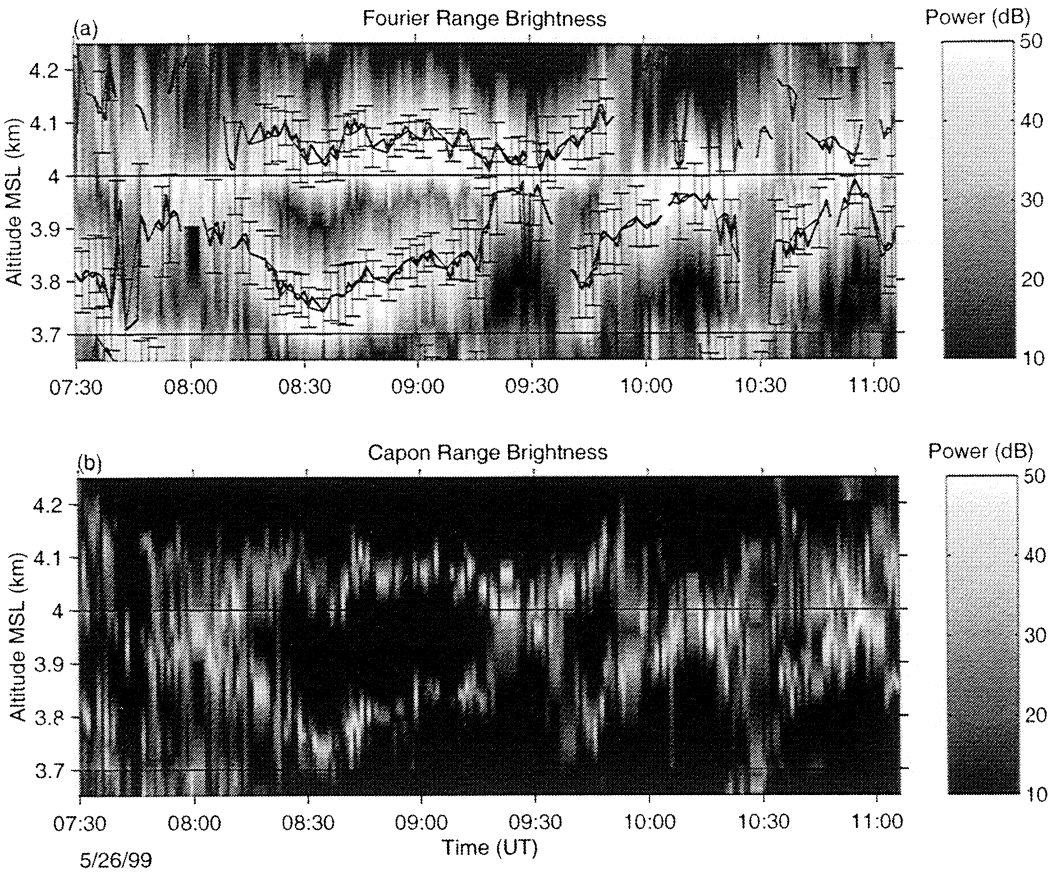

Figure 3. Comparison of (a) standard two-frequency FDI (solid line with error bars representing layer thickness), Fourier RIM and (b) Capon RIM results for a 600-m range over a 3.5-hour period on May 26, 1999. No incoherent integration was performed, providing a temporal resolution of approximately 1 min. Again, horizontal lines denote gate boundaries. A superimposed wavelike structure is seen from the Capon RIM results with a temporal period and amplitude of approximately 1 hour and 200-300 m, respectively. Although useful, two-frequency FDI analysis alone does not show the complete structure of the phenomenon.

to possess a period of slightly less than 1 hour and amplitude of approximately 200-300 m. After approximately 1030 UT the coherent structure evolves into a much shorter period, chaotic feature, possibly signifying a breakdown of the wave.

Previous results obtained by two-frequency FDI have cast doubt on the layer position estimates mainly because of potential range sidelobe leakage. Further, previous experimental results have occasionally shown the estimated layer structure to possess an unnatural periodicity in height [*Palmer et al.*, 1990]. To test this problem for the RIM case, the discrete Fourier transform of the power-weighted range brightness estimates has been calculated with respect to the range variable r_I for each profile shown in Figure 2. A similar technique is used in our companion paper for geophysical interpretation [*Chilson et al.*, this issue]. As stated previously, r_I is scanned every 5 m, providing more than adequate sampling in altitude. The spatial spectrograms resulting from both Fourier and Capon RIM analysis are provided in Figure 4. The ordinate of the figure is vertical wavenumber with the 2π dependence removed for convenience. The horizontal, white lines are placed at a value corresponding to a scale of 300 m, where a dominant feature might be expected owing to the 300-m gate spacing. Since there is no obvious peak in the spectrogram for this wavenumber, it can be assumed that the range sidelobe leakage seen in some two-frequency FDI results is not a concern for RIM

analysis, in this case. More importantly, the spectrogram can be used to deduce dominant vertical wavelengths due to the atmosphere and revealed by RIM. For example, before the occurrence of the wind maximum at 1200 UT on May 25, the power in the spectrogram is spread more uniformly over the range of wavenumbers shown in the plot. The wind maximum is not only coincident with a reduction in echo power (Figure 2a) but also seems to produce a significant effect on the spectrogram. Spectral analysis of the range brightness using RIM should prove to be a major advantage of this technique.

Now that it has been established, for this case, that Capon RIM has superior performance and is free from gate leakage biases, intriguing regions of the data set will be more closely examined. Using a single record for each estimate of range brightness, results from the Capon RIM technique are shown in Figure 5 for a 3.5-hour period beginning at 1730 UT on May 24, 1999. The altitude range is 2.15-3.65 km msl; the original gate boundaries are emphasized by horizontal lines. Again, the RIM procedure sampled at 5 m, providing 60 subgates in each 300-m gate. Although not quantified precisely, the variation in layer thickness can be examined from these data. A layer is seen in the lowest gate from 1730-1830 UT with thickness of approximately 30-50 m, based solely on the visual inspection of the range

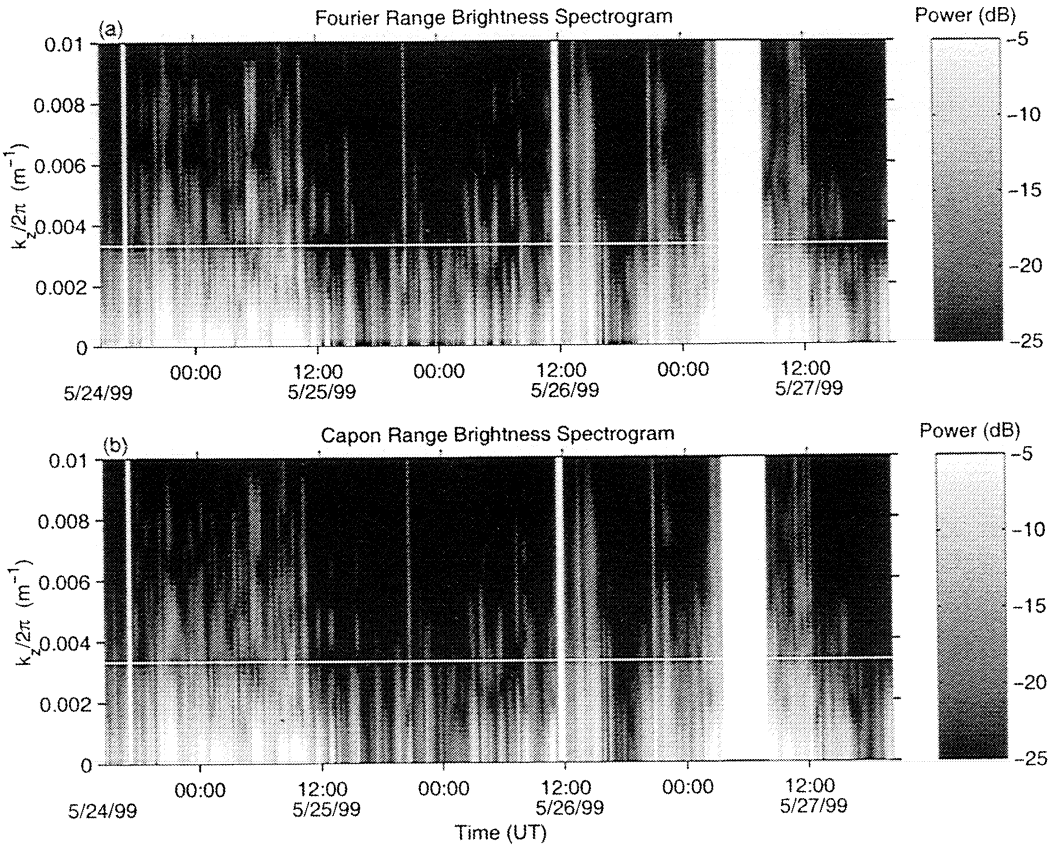

Figure 4. Spectrogram of the vertical structure produced from the (a) Fourier and (b) Capon RIM analyses over the extent of the experiment. The horizontal, white lines denote the vertical wavenumber corresponding to a layer separation of 300 m. Since there is no obvious peak in the spectrogram at $k_z/2\pi=1/300$ m^{-1}, the results of the RIM analysis can be reliably used to extract dominant vertical wavelengths, for example. Previous results using two-frequency FDI analysis have occasionally shown a periodicity related to the gate spacing, which was explained by leakage from neighboring gates. The spectrogram analysis shows that this is not the case for the RIM results.

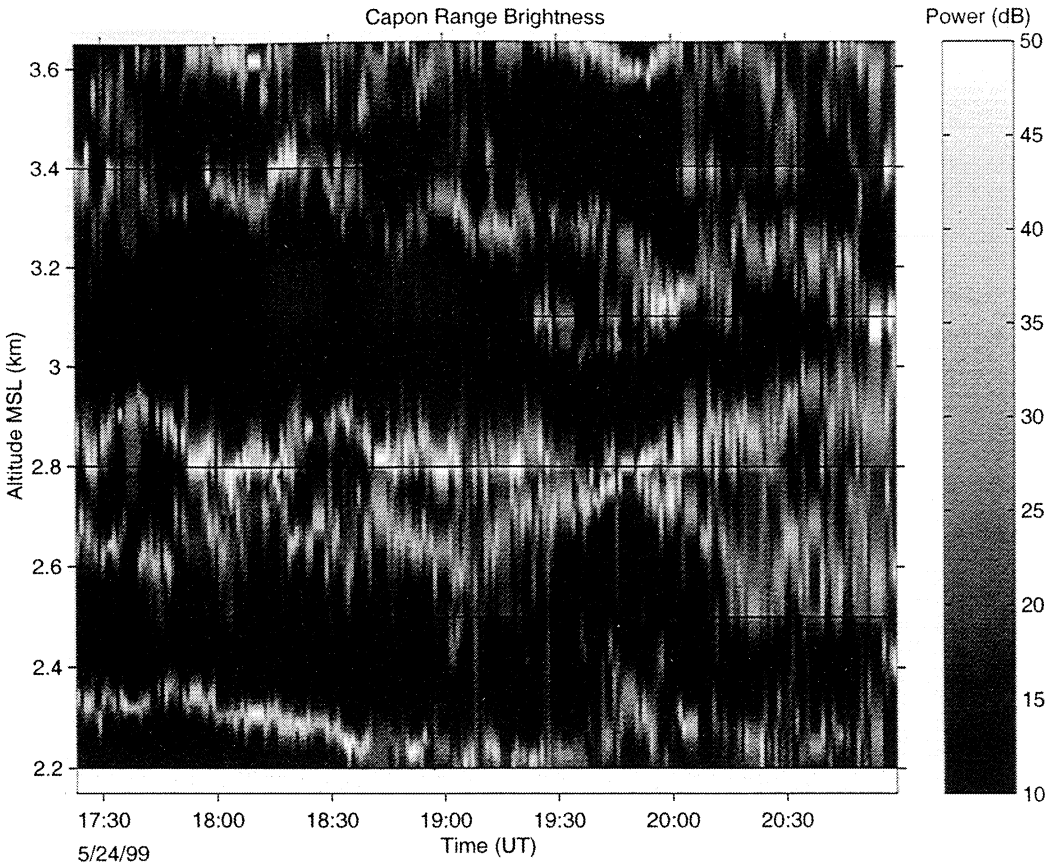

Figure 5. Capon RIM results for an approximate 3.5-hour time period with 1-min temporal resolution on May 24, 1999. Notice the wavelike structure with temporal periods as short as 20-30 min, which is reasonable given the expected Brunt-Väisälä frequency in the troposphere.

brightness plots. In the gate centered at 2.65 km msl after 2000 UT a comparably thin layer is seen to increase in thickness to a scale where it encompasses the entire gate. Another interesting short-period oscillation is observed at an altitude of 3.35 km msl at 1830 UT. Under close scrutiny a period of approximately 20-30 min is observed, which is comparable to values of the Brunt-Väisälä period shown in the companion paper [*Chilson et al.*, this issue].

A final example of the 1-min resolution Capon RIM results is shown in Figure 6. Again, a 1.5-km region is examined but from 2.45-3.95 km msl for approximately 3.5 hours immediately following the wind maximum. An apparent downward motion is observed in the layered structure shown in Figure 6. In particular, the layer observed in the upper middle portion of the plot can be seen to subside at a rate of approximately 5-8 cm s^{-1}. Possible explanations for this phenomenon include the horizontal advection of a warm front or large-scale subsidence due to a high-pressure region [*Muschinski et al.*, 1999].

5. Conclusions

This study provides an overview of the results from an implementation of RIM on the SOUSY VHF radar in Germany. This radar was chosen for this experiment, in part, because the switching capability of the transmitter frequency is extremely flexible and because it was used for previous two-frequency FDI experiments [e.g., *Chilson and Schmidt*, 1996]. The SOMARE-99 experiments, which took place in May 1999, provided an extended data set with which to test the recently proposed RIM method [*Palmer*

et al., 1999; *Luce et al.*, 2001]. Fortunately, the meteorological conditions during the campaign included a distinct wind maximum of approximately 30 m s^{-1} and intense scattering layers throughout the troposphere before and after the wind maximum. These layers were readily identified by using Capon RIM and tracked through several 300-m range gates.

Unlike two-frequency FDI analysis, RIM can theoretically be used to observe several layers within a single range gate. Under ideal conditions (high signal-to-noise ratio (SNR) and extremely thin layers) the number of layers is limited to one less than the number of frequencies used in the analysis [*Palmer et al.*, 1999]. Under more realistic conditions, however, the number of layers can often be less than three depending on the layer thicknesses, proximity, and SNR. As an example, the data presented here seldom exhibit more than two distinct layers in a single scattering volume, which could be caused by either an actual lack of multiple layers or limitations of the technique. In its present form, it may not be possible for RIM to be used to determine the true cause under all conditions. An important benefit of RIM analysis is that no assumptions about the shape of the scattering layers are needed. Interesting reflectivity structures modulated by possible gravity wave activity, which would have been unobserved with standard radar techniques, were revealed in the data. Systematic periodicities in the estimated range brightness distribution were shown to be nonexistent, providing further confidence in the method. Finally, two specific examples of high-resolution RIM results were presented, showing (1) short-period wavelike oscillations (Figure 5) and (2) apparent downward motion possibly due to the passage of a warm front or large-scale subsidence (Figure 6). Both examples showed

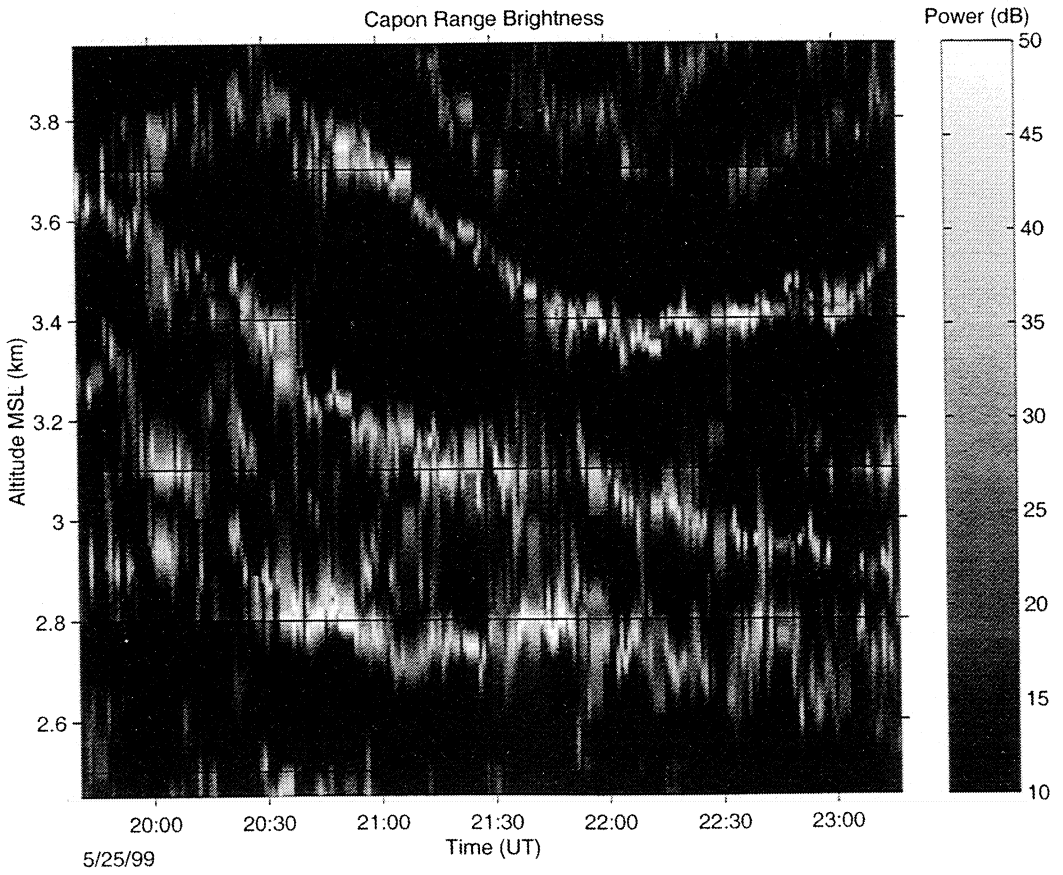

Figure 6. Same as Figure 5, except for May 25, 1999, and a different height range. Scattering layers are observed in this region with apparent downward motion of approximately 5-8 cm s^{-1}.

that Capon RIM, in particular, is a robust and useful method of observing the small-scale structures of the atmosphere.

Acknowledgments. R.D.P. and T.Y.Y. were supported by the Division of Atmospheric Sciences of the National Science Foundation through grant ATM 99-08616. P.B.C. was supported by the Environment and Space Research Institute (MRI) in Kiruna, Sweden.

References

Capon, J., High-resolution frequency-wavenumber spectrum analysis, *Proc. IEEE*, *57*(8), 1408–1419, 1969.

Chilson, P. B., and G. Schmidt, Implementation of frequency domain interferometry at the SOUSY VHF radar: First results, *Radio Sci.*, *31*, 263–272, 1996.

Chilson, P. B., A. Muschinski, and G. Schmidt, First observations of Kelvin-Helmholtz billows in an upper level jet using VHF frequency domain interferometry, *Radio Sci.*, *32*, 1149–1160, 1997.

Chilson, P. B., R. D. Palmer, A. Muschinski, D. Hooper, G. Schmidt, and H. Steinhagen, SOMARE-99: A demonstrational field campaign for ultrahigh resolution VHF atmospheric profiling using frequency diversity, *Radio Sci.*, this issue.

Czechowsky, P., G. Schmidt, and R. Rüster, The mobile SOUSY Doppler radar: Technical design and first results, *Radio Sci.*, *19*, 441–450, 1984.

Dalaudier, F., D. Sidi, M. Crochet, and J. Vernin, Direct evidence of "sheets" in the atmospheric temperature field, *J. Atmos. Sci.*, *51*(2), 237–248, 1994.

Doviak, R. J., and D. S. Zrnić, Reflection and scatter formula for anisotropically turbulent air, *Radio Sci.*, *19*, 325–336, 1984.

Franke, S. J., Pulse compression and frequency domain interferometry with a frequency-hopped MST radar, *Radio Sci.*, *25*, 565–574, 1990.

Gossard, E. E., D. R. Jensen, and J. H. Richter, An analytical study of tropospheric structure as seen by high-resolution radar, *J. Atmos. Sci.*, *28*, 794–807, 1971.

Hooper, D. A., Signal and noise level estimation for narrow spectral width returns observed by the Indian MST radar, *Radio Sci.*, *34*, 859–870, 1999.

Hysell, D. L., Radar imaging of equatorial *F* region irregularities with maximum entropy interferometry, *Radio Sci.*, *31*, 1567–1578, 1996.

Johnson, D. H., and D. E. Dudgeon, *Array Signal Processing*, Prentice-Hall, Englewood Cliffs, N. J., 1993.

Kudeki, E., and G. R. Stitt, Frequency domain interferometry: A high-resolution radar technique for studies of atmospheric turbulence, *Geophys. Res. Lett.*, *14*, 198–201, 1987.

Kudeki, E., and F. Sürücü, Radar interferometric imaging of field-aligned plasma irregularities in the equatorial electrojet, *Geophys. Res. Lett.*, *18*, 41–44, 1991.

Luce, H., M. Crochet, F. Dalaudier, and C. Sidi, Interpretation of VHF ST radar vertical echoes from in situ temperature sheet observations, *Radio Sci.*, *30*, 1003–1025, 1995.

Luce, H., M. Crochet, and C. Hanuise, On the interpretation of the layered structures detected by mesosphere-stratosphere-troposphere radar in dual frequency domain interferometry mode, *Radio Sci.*, *34*, 1077–1083, 1999.

Luce, H., M. Yamamoto, S. Fukao, D. Helal, and M. Crochet, A frequency radar interferometric imaging applied with high resolution methods, *J. Atmos. Sol. Terr. Phys.*, *63*, 221–234, 2001.

Muschinski, A., and C. Wode, First in situ evidence for coexisting submeter temperature and humidity sheets in the lower free troposphere, *J. Atmos. Sci.*, *55*, 2893–2906, 1998.

Muschinski, A., P. B. Chilson, S. Kern, J. Nielinger, G. Schmidt, and T. Prenosil, First frequency-domain interferometry observations of large-scale vertical motion in the atmosphere, *J. Atmos. Sci.*, *56*, 1248–1258, 1999.

Muschinski, A., R. Frehlich, M. Jensen, R. Hugo, A. Hoff, F. Eaton, and B. Balsley, High-resolution measurements of atmospheric turbulence above the surface layer: An intercomparison between a kite- and blimp-borne and a helicopter-borne turbulence measurement system, *Boundary Layer Meteorol.*, *98*, 219–250, 2001a.

Muschinski, A., P. B. Chilson, R. D. Palmer, G. Schmidt, and H. Steinhagen, Boundary-layer convection and diurnal variation of vertical-velocity characteristics in the free troposphere, *Q. J. R. Meteorol. Soc.*, *127*, 423–444, 2001b.

Palmer, R. D., R. F. Woodman, S. Fukao, M. F. Larsen, M. Yamamoto, T. Tsuda, and S. Kato, Frequency domain interferometry observations of tropo/stratospheric scattering layers using the MU radar: Description and first results, *Geophys. Res. Lett.*, *17*, 2189–2192, 1990.

Palmer, R. D., S. Gopalam, T. Yu, and S. Fukao, Coherent radar imaging using Capon's method, *Radio Sci.*, *33*, 1585–1598, 1998.

Palmer, R. D., T.-Y. Yu, and P. B. Chilson, Range imaging using frequency diversity, *Radio Sci.*, *34*, 1485–1496, 1999.

Petitdidier, M., A. Sy, A. Garrouste, and J. Delcourt, Statistical characteristics of the noise power spectral density in UHF and VHF wind profilers, *Radio Sci.*, *32*, 1229–1247, 1997.

Richter, J. H., High resolution tropospheric radar sounding, *Radio Sci.*, *4*, 1261–1268, 1969.

Röttger, J., and G. Schmidt, High-resolution VHF radar sounding of the troposphere and stratosphere, *IEEE Trans. Geosci. Electron.*, *17*, 182–189, 1979.

Schmidt, G., R. Rüster, and P. Czechowsky, Complementary code and digital filtering for detection of weak VHF radar signals from the mesosphere, *IEEE Trans. Geosci. Electron.*, *17*, 154–161, 1979.

Thompson, A. R., *Interferometry and Synthesis in Radio Astronomy*, John Wiley, New York, 1986.

Woodman, R. F., Spectral moment estimation in MST radars, *Radio Sci.*, *20*, 1185–1195, 1985.

Woodman, R. F., Coherent radar imaging: Signal processing and statistical properties, *Radio Sci.*, *32*, 2373–2391, 1997.

Yu, T.-Y., R. D. Palmer, and D. L. Hysell, A simulation study of coherent radar imaging, *Radio Sci.*, *35*, 1129-1141, 2000.

P. B. Chilson and A. Muschinski, NOAA Environmental Technology Laboratory, Cooperative Institute for Research in Environmental Sciences (CIRES), University of Colorado-NOAA, 325 Broadway, R/ET4, Boulder, CO 80303-3328. (pchilson@etl.noaa.gov; amuschinski@etl.noaa.gov)

R. D. Palmer, Department of Electrical Engineering, University of Nebraska, Lincoln, NE 68588-0511. (bpalmer@unl.edu)

G. Schmidt, Max-Plank-Institut für Aeronomie, Lindau, Germany. (gschmidt@linax1.mpae.gwdg.de)

H. Steinhagen, Meteorologisches Observatorium Lindenberg, Am Observatorium 12, D-15864 Lindenberg, Germany. (hans.steinhagen@dwd.de)

T.-Y. Yu, National Center for Atmospheric Research, Atmospheric Technology Division, Boulder, CO 80301-2260. (tianyou@atd.ucar.edu)

(Received Dec. 21, 1999; revised Sept. 14, 2000; accepted Sept. 25, 2000.)